

ORIGINAL ARTICLE

## DNA damage and oxidative stress induced by CeO<sub>2</sub> nanoparticles in human dermal fibroblasts: Evidence of a clastogenic effect as a mechanism of genotoxicity

Laila Benameur<sup>1,2</sup>, Mélanie Auffan<sup>3,4</sup>, Mathieu Cassien<sup>1</sup>, Wei Liu<sup>2,3</sup>, Marcel Culcasi<sup>1</sup>, Hidayat Rahmouni<sup>1</sup>, Pierre Stocker<sup>1</sup>, Virginie Tassistro<sup>2</sup>, Jean-Yves Bottero<sup>3,4</sup>, Jérôme Rose<sup>3,4</sup>, Alain Botta<sup>2,4</sup>, and Sylvia Pietri<sup>1</sup>

<sup>1</sup>Aix-Marseille Université, CNRS, Institut de Chimie Radicale UMR 7273, Equipe Sondes Moléculaires en Biologie et Stress Oxydant, Marseille, France, <sup>2</sup>Aix-Marseille Université, CNRS, IMBE UMR 7263, Marseille, France, <sup>3</sup>Aix-Marseille Université, CNRS, CEREGE UMR 7330, Aix-en-Provence, France, and <sup>4</sup>International Consortium for the Environmental Implications of Nanotechnology iCEINT, Aix-en-Provence, France

### Abstract

The broad range of applications of cerium oxide (CeO<sub>2</sub>) nanoparticles (nano-CeO<sub>2</sub>) has attracted industrial interest, resulting in greater exposures to humans and environmental systems in the coming years. Their health effects and potential biological impacts need to be determined for risk assessment. The aims of this study were to gain insights into the molecular mechanisms underlying the genotoxic effects of nano-CeO<sub>2</sub> in relation with their physicochemical properties. Primary human dermal fibroblasts were exposed to environmentally relevant doses of nano-CeO<sub>2</sub> (mean diameter, 7 nm; dose range,  $6 \times 10^{-5}$ – $6 \times 10^{-3}$  g/l corresponding to a concentration range of 0.22–22  $\mu$ M) and DNA damages at the chromosome level were evaluated by genetic toxicology tests and compared to that induced in cells exposed to micro-CeO<sub>2</sub> particles (mean diameter, 320 nm) under the same conditions. For this purpose, cytokinesis-blocked micronucleus assay in association with immunofluorescence staining of centromere protein A in micronuclei were used to distinguish between induction of structural or numerical chromosome changes (*i.e.* clastogenicity or aneuploidy). The results provide the first evidence of a genotoxic effect of nano-CeO<sub>2</sub>, (while not significant with micro-CeO<sub>2</sub>) by a clastogenic mechanism. The implication of oxidative mechanisms in this genotoxic effect was investigated by (i) assessing the impact of catalase, a hydrogen peroxide inhibitor, and (ii) by measuring lipid peroxidation and glutathione status and their reversal by application of *N*-acetylcysteine, a precursor of glutathione synthesis in cells. The data are consistent with the implication of free radical-related mechanisms in the nano-CeO<sub>2</sub>-induced clastogenic effect, that can be modulated by inhibition of cellular hydrogen peroxide release.

### Keywords

Cytokinesis-blocked micronucleus assay, free radicals, glutathione status, nanoceria, nanogenotoxicity

### History

Received 6 September 2013  
Revised 20 August 2014  
Accepted 21 September 2014  
Published online 17 October 2014

### Introduction

Nanomaterials have a wide variety of potential applications in many fields including catalysis, biomedicine and engineering. They currently attract intense research efforts due to the unusual behavior and physicochemical properties of nanoscale materials compared to their bulk counterparts. However, concerns regarding their potential hazardous effects on human health and environment prompted a proactive approach to ensuring the safety and sustainability of emerging nanotechnology (Auffan et al., 2009a; Nel et al., 2006; Wiesner et al., 2006). Engineered cerium oxide (CeO<sub>2</sub>) nanoparticles, nanoceria (nano-CeO<sub>2</sub>) are considered as some of the most interesting metal oxide nanoparticles for industrial purposes in the fields of catalysis

(Campbell & Peden 2005; Park et al., 2007), due to the occurrence of both enhanced dioxygen exchange and Ce<sup>3+</sup>/Ce<sup>4+</sup> redox cycling (Campbell & Peden, 2005; Esch et al., 2005). In addition, nano-CeO<sub>2</sub> has been extensively applied as oxygen sensor and high-temperature oxidation protection material (Izu et al., 2004; Jasinski et al., 2003; Patil et al., 2002), fuel additive to improve the efficiency of combustion (Park et al., 2007), redox nanocatalyst and detection tool in immunoassays (Asati et al., 2009), and sensitive dosimeter for low radiation (Li et al., 2009).

Given the increasing range of applications of nanomaterials, which can easily enter the body by many routes, there is a debate about whether nanoparticles may exert long-term toxicity (occupational or environmental), in particular via inhalation or dermal contact (Stern & McNeil, 2008). Among the possible ways by which nanomaterials could be toxic to cells, oxidative stress has been found to occur in the case of nanoparticles from various metal oxides (*e.g.* CuO or TiO<sub>2</sub>), fullerenes and single-walled carbon tubes (Karlsson et al., 2008; Long et al., 2006; Sayes et al., 2005; Sharma et al., 2007). Several studies have documented the oxidative stress-mediated toxicity of nano-CeO<sub>2</sub> in many cell

Correspondence: Dr Laila Benameur, Faculté des Sciences de Saint-Jérôme, CNRS, ICR UMR 7273, Equipe Sondes Moléculaires en Biologie et Stress Oxydant, Aix-Marseille Université, Case 522, Avenue Escadrille Normandie Niemen, 13397 Marseille Cedex 20, France. Tel: +0033 660 15 92 46. E-mail: laila.benameur@gmail.com

types such as *Escherichia coli* (Thill et al., 2006), *Pseudokirchneriella subcapitata* (Rogers et al., 2010), *Caenorhabditis elegans* (Zhang et al., 2011), human lung cancer cells (Lin et al., 2006), human bronchial epithelial cells (Eom & Choi, 2009; Park et al., 2008), and human hepatoma cells (Cheng et al., 2013). However, due to some of its apparent antioxidant effects nano-CeO<sub>2</sub> is still considered a relatively safe nanomaterial (Culcasi et al., 2012).

The recent observation that exposing various cell systems to nano-CeO<sub>2</sub> induced over expression of apoptosis and DNA fragmentation (Hussain et al., 2012), autophagy and inflammation (Cho et al., 2010; Ma et al., 2012) suggested genotoxicity as a possible consequence of nano-CeO<sub>2</sub>-induced oxidant stress. Indeed, reactive oxygen species (ROS) such as hydroxyl radical (HO<sup>•</sup>) can lead to DNA strand breaks, base and sugar lesions, and DNA cross-links, all of which having the potential to initiate and promote carcinogenesis (Singh et al., 2009; Valko et al., 2006). A more direct approach sustaining nano-CeO<sub>2</sub>-induced genotoxicity was provided by Auffan et al. (2009b) and De Marzi et al. (2013) who used the comet assay in different cell lines challenged with the nanoparticles.

The role of ROS in the toxic effects of nano-CeO<sub>2</sub> was recently confirmed by electron spin resonance (ESR) spectrometry and spectrophotometric techniques which allowed to identify Nox2- and Nox4-dependent NADPH oxidase complexes, and the mitochondria as cellular sources of superoxide (O<sub>2</sub><sup>-</sup>)/hydrogen peroxide (H<sub>2</sub>O<sub>2</sub>) formation in dermal fibroblasts exposed to various concentrations of the particles (Culcasi et al., 2012). Since this cell-nanoparticle interaction also triggered an extracellular release of ascorbate (Culcasi et al., 2012), HO<sup>•</sup> could be formed secondarily by Fenton-type reactions, giving a mechanistic basis for nano-CeO<sub>2</sub>-induced genotoxicity.

In this paper, we investigated in more details the mechanisms underlying the promotion of DNA damage to primary culture of human dermal fibroblasts by environmentally relevant concentrations (at the micromolar range) of nano-CeO<sub>2</sub>. We used the cytokinesis-blocked micronucleus (CBMN) assay associated with immunofluorescence staining of centromere protein A (CENP-A) in micronuclei. The main advantage of the CBMN assay is its ability to elucidate the genotoxic mechanism of substances with clastogenic or aneugenic modes of action (Albertini et al., 2000; Benameur et al., 2011; Kirsch-Volders et al., 2002; Mateuca et al., 2006). In addition, we evaluated the specificity of nano-CeO<sub>2</sub> versus micro-CeO<sub>2</sub> particles having ~50-fold higher mean size to favor genotoxicity and increase oxidative stress (i.e. cell lipid peroxidation and depletion of glutathione levels). Finally, using X-ray absorption spectroscopy, we assessed if the release of ascorbate by cells could be involved in structural changes at the surface of nano-CeO<sub>2</sub>. The data provide the first evidence for a H<sub>2</sub>O<sub>2</sub> production-related clastogenic mechanism to explain the genotoxicity of nano-CeO<sub>2</sub> in human dermal fibroblasts.

## Methods

### Reagents

All reagents for cell cultures including phosphate-buffered saline (PBS) and Dulbecco's modified Eagle's medium (DMEM) were provided by PAA Laboratories (Linz, Austria). Mitomycin C, colchicine, cytochalasin-B, paraformaldehyde, Triton<sup>®</sup> X-100, phalloidin-tetramethylrhodamine B isothiocyanate, bovine serum albumin (BSA), 1,1,3,3-tetramethoxypropane (TMP), 2-thiobarbituric acid (TBA), *N*-acetylcysteine (NAC) and bovine liver catalase were from Sigma-Aldrich (Saint Quentin Fallavier, France) and 4'-6-diamidino-2-phenylindole (DAPI) was provided by ICN (Orsay, France). CENP-A primary antibody (ab13939) was from Abcam (Cambridge, UK) and cyanine

3-conjugated secondary antibody (M35010) was from Invitrogen (Cergy-Pontoise, France).

### CeO<sub>2</sub> nano- and micro-particles

Nano-CeO<sub>2</sub> (Rhodia Chemicals, Courbevoie, France) was synthesized by aqueous precipitation of Ce<sup>4+</sup>(NO<sub>3</sub>)<sub>4</sub> salt at acidic pH (Nabavi et al., 1993; Spalla & Cabane, 1993). The composition of the precipitate is CeO<sub>2</sub>(HNO<sub>3</sub>)<sub>0.5</sub>(H<sub>2</sub>O)<sub>4</sub>. These nanoparticles are ellipsoidal crystallites of cerianite with a mean diameter of 7 nm and a specific surface area (SSA) of 400 m<sup>2</sup>/g (Auffan et al., 2009b; Spalla & Cabane 1993; Thill et al., 2006). Powdered micro-CeO<sub>2</sub>, obtained by calcinations and grindings, are crystallites of cerianite, with a mean diameter of 320 nm and a SSA estimated from the mean size at ~40 m<sup>2</sup>/g (Auffan et al., 2009b). The detailed structural characterization of nano- and micro-CeO<sub>2</sub> particles in water and culture media is given in the Supporting Material section (Figure 6 of Supplementary material 1). The colloidal stabilities over time of CeO<sub>2</sub> particles in water and DMEM were estimated by dynamic light scattering (DLS) using a Zetasizer Nano ZS analyzer (Malvern Instruments, Orsay, France). The determination of zeta potentials of particles in water as a function of pH and in DMEM at pH 7.35 was performed as previously described (De Faria & Trasatti, 1994; Nabavi et al., 1993).

### Normal human fibroblast culture

Primary cultures of normal human fibroblasts were isolated by the outgrowth method using infant foreskins obtained after circumcision (Nahm et al., 2002). The dermis was cut into small pieces of 0.5–1 mm<sup>3</sup> under sterile conditions. The small tissue pieces were seeded in culture dishes and incubated in DMEM containing 10% fetal calf serum, L-glutamine (2 mM), sodium pyruvate (1 mM), penicillin (100 U/ml) and streptomycin (100 µg/ml). Fibroblasts were then cultured at 37 °C in complete, antibiotic-free DMEM in a 5% CO<sub>2</sub> humidified atmosphere. The isolated fibroblasts were obtained after two weeks and the culture medium was changed every two days.

### CBMN assay

CBMN assay was carried out to determine genotoxic potential of nano-CeO<sub>2</sub>. Normal human fibroblasts were seeded into four-well chamber slides at a density of 1–5 × 10<sup>4</sup> cells per well and cultured in complete culture medium for 24 h at 37 °C. In the following experiments, the cells were then treated with assay medium containing the tested compounds. All assays were performed in three independent experiments as recommended (Kirsch-Volders et al., 2003) and for each assay at least two wells per treatment were analyzed. The cells were then incubated for 48 h with a stable colloidal suspension of either nano-CeO<sub>2</sub> or micro-CeO<sub>2</sub> at a dose ranging 6 × 10<sup>-5</sup>–6 × 10<sup>-3</sup> g/l (i.e. 0.22–22 µM) in DMEM. In a series of inhibition experiments, cells were co-exposed with nano-CeO<sub>2</sub> and the H<sub>2</sub>O<sub>2</sub> scavenger catalase at 500 U/ml, a concentration which was found effective in protecting cells from apoptosis (Katschinsky et al., 2000). Wells containing DMEM only were taken as negative controls. In two randomly selected wells, the cells were incubated for 48 h at 37 °C in the presence of either mitomycin C (10 ng/ml) or colchicine (25 nM) as clastogenic and aneugenic positive control agents, respectively.

In each treated or control wells, cytochalasin-B (2 µg/ml) was added after the first 24 h incubation to block the cytokinesis, thus cells that have undergone one nuclear division are recognized by their binucleate appearance. At the end of the 48 h exposure protocol, various particles and reagents were removed and the cells were reincubated with fresh DMEM for 2 h at 37 °C. After removal of the incubation medium the cells were washed

twice in calcium- and magnesium-free PBS, immediately fixed for 10 min with PBS containing 4% paraformaldehyde, washed with plain PBS and reincubated for 10 min in PBS containing 0.5% Triton X-100. Actin staining was performed over 30 min with phalloidin-tetramethylrhodamine B isothiocyanate (0.06 µg/ml) in PBS. Cells were washed twice for 2 min in PBS containing 0.5% Triton X-100. The medium was removed and DAPI (0.1 µg/ml in PBS) was added for 10 min to counterstain DNA. After removal of the medium, cells were washed in PBS for 2 min and the stained slides were mounted in an antifade agent Vectashield H-1000 (Vector Labs., Burlingame, CA), coded and scored blindly by a single investigator with an epifluorescence microscope (BX 60 Olympus, Rungis, France) at 400× magnification. Micronuclei (MN) were assessed in binucleated cells (BNC) that had completed nuclear division after exposure. For each tested particle concentration, 1000 BNC with a well-preserved cytoplasm were examined, and the number of binucleated micronucleated cells was scored per 1000 BNC. Identification and criteria for scoring of MN were as described (Fenech, 2007).

Five-hundred cells were analyzed for the presence of cells that were mono-, bi-, tri- and tetranucleated, using DAPI fluorescence. The cytokinesis block proliferation index (CBPI) provides the average number of cell divisions, completed by the cell, and it was calculated as described (Kirsch-Volders et al., 2003).

### CENP-A analysis

To evaluate the mechanistic origin of individual micronuclei, the contents of micronuclei were investigated using immunofluorescence staining of CENP-A in association with the CBMN assay. This approach served to distinguish between clastogenic and aneugenic effects induced by nano-CeO<sub>2</sub> in condition of presence or absence of catalase. The CENP-A analysis was performed as described by Benameur et al. (2011). Cells were washed three times with PBS, incubated for 5 min with a solution of 0.5% Triton X-100 in PBS, and incubated for 15 min in 1% BSA/PBS at room temperature. The anti-CENP-A primary antibody (1:200 in 1% BSA/PBS) was incubated for 3 h at 37 °C. Then, cells were washed and incubated for 1 h with cyanine 3-conjugated secondary antibody (1:40 in 1% BSA/PBS) at room temperature. Then, cells were washed with PBS, incubated for 5 min in DAPI (0.1 µg/ml) and washed in plain PBS for 2 min. After being stained, the slides were mounted as indicated above, and analyzed at 400× magnification or oil immersion 1000× magnification. All assays were performed in three independent experiments done in duplicates. For each assay, 1000 binucleated cells were scored, the MN in BNC examined for the presence of one or more fluorescent signals, and classified as centromere positive (C+MN; i.e. CENPA-positive MN; aneugenic effect) or centromere negative (C-MN; i.e. CENPA-negative MN; clastogenic effect). The same scoring criteria as described above for the MN assay were applied (Fenech, 2007).

### Malondialdehyde-thiobarbituric acid assay

In another set of experiments, isolated fibroblasts (10<sup>5</sup> cells/ml) were plated in 25 cm<sup>2</sup> flasks in a humidified atmosphere of 5% CO<sub>2</sub> in air as previously described (Culcasi et al., 2012). Cells were then incubated for 48 h in DMEM containing a suspension of either nano-CeO<sub>2</sub> or micro-CeO<sub>2</sub> (6 × 10<sup>-5</sup>–6 × 10<sup>-3</sup> g/l). In experiments with nano-CeO<sub>2</sub>, a set of inhibition assays were performed where either catalase (500 U/mL) or NAC (2 mM) were added to the medium. When catalase was used, it was co-incubated with the nano-CeO<sub>2</sub>-treated cells. In experiments involving NAC, the compound was first added to DMEM for 24 h (pretreatment phase), the milieu was removed and cells were resuspended with fresh DMEM containing NAC and particles,

and the mixture was incubated for 48 h. At the end of the exposure period, cells were washed in calcium- and magnesium-free PBS, trypsinized and resuspended in PBS to reach ~50,000 cells/ml.

Lipid peroxidation was assessed by measuring cellular *Malondialdehyde-thiobarbituric acid* (MDA-TBA) content in 0.5 ml of trypsinized cells, which were homogenized in 1.5 ml of 1.15% KCl solution and centrifuged for 10 min at 4 °C (1000 × g). The MDA-TBA content of the supernatant was determined as previously described (Culcasi et al., 2006). In brief, 1 ml of the cell homogenate supernatant, treated with 0.5 ml acetic acid (20%) and 0.5 ml TBA (10 g/l), was incubated for 20 min at 95 °C, cooled and MDA-TBA was assayed at 532 nm. A calibration curve was obtained from standard MDA-TBA samples prepared by using 0.25 ml aliquots of 0.1–10 mM TMP solutions. Proteins were determined by the method of Lowry et al. (1951) in two randomly selected flasks. MDA-TBA analyses were representative of 6 independent experiments made in duplicate.

### Reduced glutathione (GSH)/oxidized glutathione (GSSG) determination

Additional 25 cm<sup>2</sup> flasks of isolated fibroblasts (10<sup>5</sup> cells/ml) were incubated at 37 °C under the same conditions, CeO<sub>2</sub> particles and inhibitors as described above. At the end of the exposure time, cells were collected and samples consisting of ~5 × 10<sup>5</sup> cells were washed twice in ice-cold PBS (pH 7.2) and 50 mM borate buffer (pH 10.5) containing 0.5% Triton X-100 was added. An aliquot was removed for protein determination, and remaining proteins were then precipitated with 1 M perchloric acid in 0.2 M boric acid. Samples were centrifuged, and the supernatants (150 µl) were derivatized with 40 mM iodoacetic acid at pH 9.0 for 15 min. The pH was adjusted to 9.0 with KOH/tetraborate solution (150 µl). Dansyl chloride was added (10 mM final), and samples were left at room temperature for 24 h in the dark to form *S*-carboxymethyl-*N*-dansyl-GSH and *N,N*'-bis-dansyl-GSSG adducts. Unreacted dansyl chloride was extracted with chloroform and the GSH and GSSG adducts were separated by HPLC (see below) and quantified relative to standards using a fluorescence detector (excitation wavelength, 335 nm, emission wavelength, 515 nm). HPLC analysis was performed using a Waters Alliance™ System (Waters SAS, Guyancourt, France) equipped with a Waters 2690 XE separation module and a Waters 474 Scanning fluorescence detector controlled by the Waters Millennium™ Chromatography manager software. Separation was achieved at room temperature on a 3-aminopropyl column (250 mm × 4.6 mm; 5 µm; Macherey-Nagel, Hoerd, France) with an isocratic flow rate of 1.2 ml/min. Solvent A is a 0.2 M acetate buffer (pH 4.6) and solvent B is 80% (v/v) methanol/water. Quantification was based on peak area.

### XANES at the Ce L<sub>3</sub>-edge

The surface properties of nano- and micro-CeO<sub>2</sub> particles were monitored at the atomic scale by X-ray absorption near edge structure (XANES) spectra collected at the Ce L<sub>3</sub>-edge. Experiments were carried out in transmission mode on the XAFS 11.1 beamline at the ELETTRA synchrotron (Trieste, Italy; Di Cicco et al., 2009). Samples were mixed with boron nitride pressed to thin pellets, and cooled with liquid nitrogen during spectra acquisition. This procedure improves spectrum quality by minimizing radiation damages and keeping Ce in the same oxidation state during the experiment (Meitzner et al., 2005). The spectra were compiled from the merge of three scans, and the energy was calibrated using a CeO<sub>2</sub> standard reference. XANES data were obtained after performing standard procedures for pre-edge subtraction and normalization using the IFEFFIT software package (Newville, 2001).

## Statistics

All values are expressed as the means  $\pm$  standard error of mean (SEM). The Kolmogorov–Smirnov test was first applied to test for a normal distribution. Differences were then analyzed by one-way analysis of variance (ANOVA) followed, if significant, by *a posteriori* Tukey tests. Intergroup differences were considered to be significant at  $p < 0.05$ .

## Results

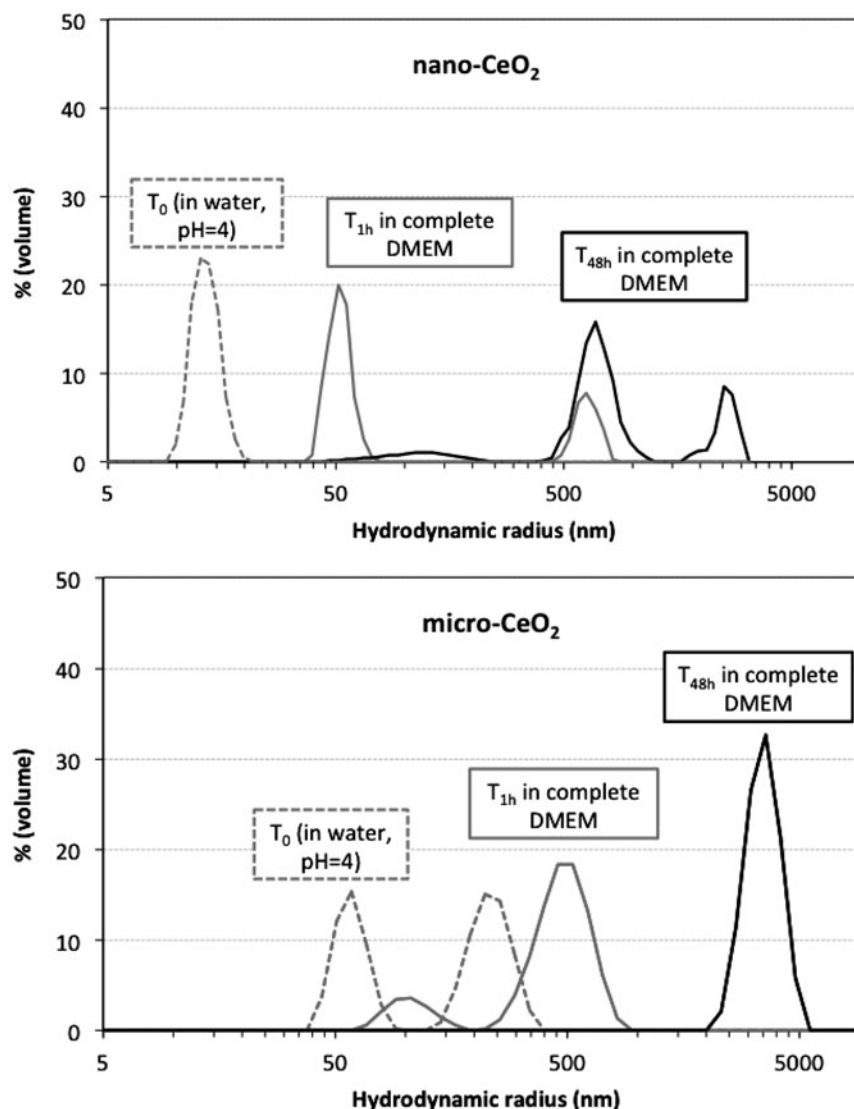
### Colloidal stability and surface charge measurements of the CeO<sub>2</sub> particles

The colloidal stability of nano- and micro-CeO<sub>2</sub> (both at  $10^{-2}$  g/l) was assessed by DLS in acidic water (pH 4) and in complete DMEM (pH 7.35) over a 48 h period. Figure 1 (upper panel) shows that nano-CeO<sub>2</sub> suspensions are stable in acidic water, with hydrodynamic diameters centered around 30 nm. The properties of these particles in acidic medium and the study of their surface chemistry were described earlier (Nabavi et al., 1993; Thill et al., 2006) and it was determined that stable solutions of perfectly dispersed nano-CeO<sub>2</sub> particles are spontaneously obtained below pH 5. The variation of the mean hydrodynamic diameter as a function of pH in water (Figure 7 of Supplementary material 2) evidenced a strong elevation in the mean hydrodynamic diameter near pH 6, steadily reaching 2500 nm at pH 7. At pH 3, the zeta

potential of nano-CeO<sub>2</sub> was of  $37 \pm 9$  mV, a positive value in agreement with earlier reports on ceria particles prepared using an acidic treatment in the last step of the process (Limbach et al., 2005; Patil et al., 2007). In such acidic medium, micro-CeO<sub>2</sub> suspensions distributed in two populations in size (mean diameters, 120 nm and 450 nm; Figure 1, lower panel), and positive zeta potentials were also obtained ( $25 \pm 3$  mV). Upon increasing the pH up to 10, both types of particles exhibited a decrease of the zeta potential toward negative values. For micro-CeO<sub>2</sub>, the point of zero charge was near pH 6.2 and values at pH 7.2 and pH 9.5 were  $-15 \pm 2$  mV and  $-25 \pm 3$  mV, respectively. Interestingly, previous studies have shown a more alkaline point of zero charge for nano-CeO<sub>2</sub> particles (i.e. in the pH 8–10 range), which still retain low positive charges at cellular pH (De Faria & Trasatti, 1994; Nabavi et al., 1993; Thill et al., 2006).

When incubation of nano-CeO<sub>2</sub> was performed for 1 h in DMEM instead of water, aggregation occurred with two populations of sizes at  $\sim 100$  nm (larger fraction) and  $\sim 1200$  nm mean diameter (Figure 1, upper panel). After 48 h incubation, the mean diameter of these two populations of aggregates increased up to 1300 nm (larger fraction) and 6000 nm. Micro-CeO<sub>2</sub> suspensions similarly underwent a rapid agglomeration in DMEM, with aggregate sizes of 1000 nm and 6000 nm after 1 h and 48 h, respectively (Figure 1, lower panel). In DMEM (pH 7.35), the zeta potential of nano-CeO<sub>2</sub> shifted to a negative value

Figure 1. Distribution of the hydrodynamic radius of nano-CeO<sub>2</sub> (upper panel) and micro-CeO<sub>2</sub> (lower panel) particles in water (pH 4) or after 1 h and 48 h of incubation in complete DMEM (pH 7.35). The particles were obtained from  $10^{-2}$  g/l CeO<sub>2</sub>.



( $-12 \pm 3$  mV) suggesting that strong interactions have occurred with proteins which affect the surface charge density. For several oxide nanoparticles, protein adsorption dominates the charge distribution, yielding negative surface densities in the range  $-10$ – $-25$  mV (Limbach et al., 2005). Although the same qualitative trend was seen in micro-CeO<sub>2</sub> (with a zeta potential of  $-19 \pm 5$  mV in DMEM), our data suggest that this negative shift of zeta potential may be better related to the pH increase than to the medium composition by itself.

Supporting Information section (Figure 7 of Supplementary material 2) includes the zeta potential studies in comparison with literature data.

### Induction of micronuclei in normal human dermal fibroblasts exposed to CeO<sub>2</sub> particles

The CBMN assay, which evaluates chromosome damage, was used to assess genotoxic response following 48 h exposure of fibroblasts at non-cytotoxic (i.e.  $6 \times 10^{-5}$ – $6 \times 10^{-4}$  g/l; 0.22–2.2  $\mu$ M) to low cytotoxic (i.e.  $6 \times 10^{-3}$  g/l; 22  $\mu$ M) doses of CeO<sub>2</sub> particles (Auffan et al., 2009b; Culcasi et al., 2012). With respect to control cells, application of nano-CeO<sub>2</sub>, even at non-cytotoxic doses, induced a statistically significant ( $p < 0.001$ ) increase of the MN frequency that was at least comparable to that seen in cells treated by either the clastogen mitomycin C (10 ng/ml) or the aneugen colchicine (25 nM; Figure 2A). In a first inhibition experiment, adding 500 U/ml catalase, a specific H<sub>2</sub>O<sub>2</sub> inhibitor, to the nano-CeO<sub>2</sub>-containing incubation medium for 48 h led to a significant ( $p < 0.01$ ) 5–8-fold decrease of the

frequency of micronucleated cells, with no dependence on the nanoparticles dose (Figure 2A). In another set of experiments, loading the cells for 48 h with micro-CeO<sub>2</sub> instead of nano-CeO<sub>2</sub> resulted in a significant ( $p < 0.01$  versus control cells) increase of MN production only at the highest tested concentration of  $6 \times 10^{-3}$  g/l, the genotoxic effect of the microparticles being yet significantly ( $p < 0.01$ ) lower than that seen with the nanoparticles (Figure 2A).

To check for non specific effects on cell division, CBPI was determined in cells incubated for 48 h under the above conditions (CeO<sub>2</sub> particles, mitomycin C, colchicine or added catalase). Compared to control cells, none of the applied compounds interfered with cell proliferation (Figure 2B).

### Assessment of the genotoxic mechanisms of CeO<sub>2</sub> nanoparticles

Micronuclei may contain (i) acentric chromosomal fragments (C-MN) formed by unrepaired double-strand breaks or by misrepair of various DNA lesions (clastogenic effect, DNA as target), or (ii) lagged entire chromosomes (C+MN) that have failed to segregate into a daughter macronucleus during the anaphase separation of mitosis (aneugenic effect, mostly non-DNA target). The clastogenic and aneugenic events lead to structural and numerical chromosomal aberrations, respectively, which are involved in birth defects and miscarriages. Thus, testing for both clastogenic and aneugenic activity of substances is highly justified (Albertini et al., 2000; Benameur et al., 2011; Kirsch-Volders et al., 2002; Mateuca et al., 2006).

Figure 2. CBMN assay on human dermal fibroblasts incubated for 48 h with 10 ng/ml mitomycin C (MMC), 25 nM colchicine (Col.), nano- or micro-CeO<sub>2</sub> ( $6 \times 10^{-5}$ – $6 \times 10^{-3}$  g/l; 0.22–22  $\mu$ M) and effect of catalase (500 U/ml) coexposure.

(A) Frequency of binucleated micronucleated cells. (B) Cytokinesis block proliferation index (CBPI). Data represent means  $\pm$  SEM of  $n = 3$  independent experiments made in duplicate. One-way ANOVA followed by Tukey test: \*\* $p < 0.01$  and \*\*\* $p < 0.001$  versus control cells (DMEM medium); † $p < 0.01$  versus cells treated with nano-CeO<sub>2</sub> alone at the same concentration.

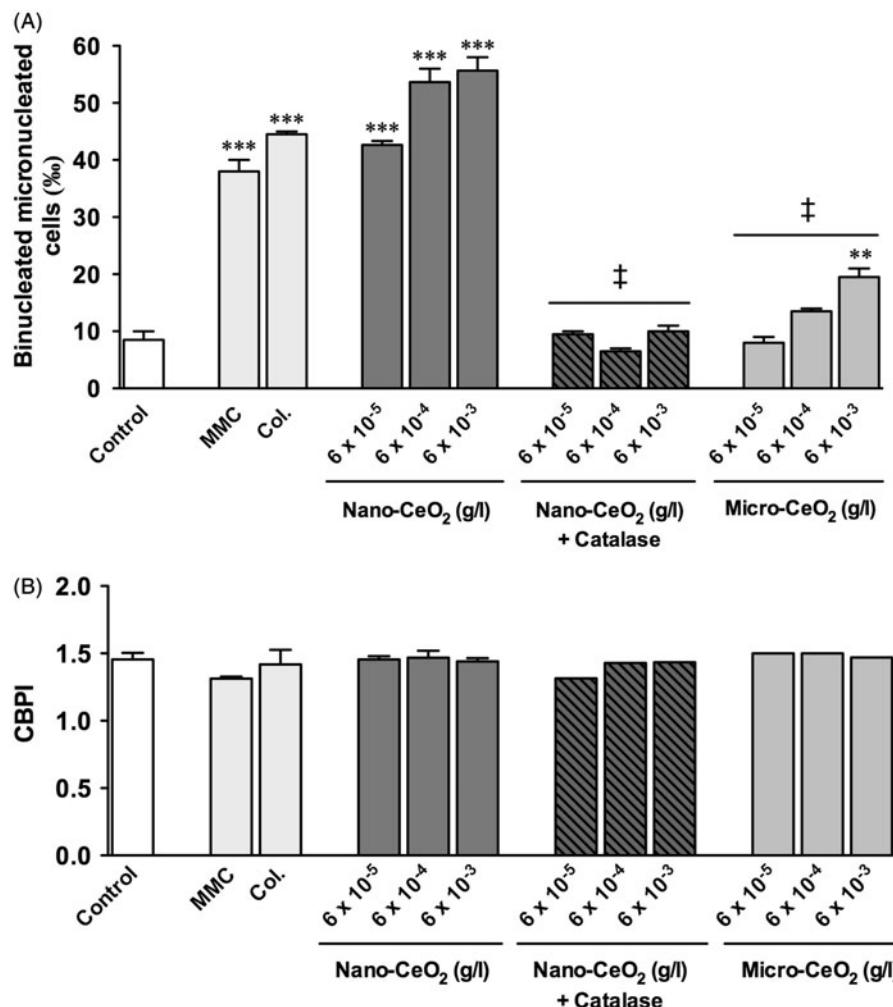
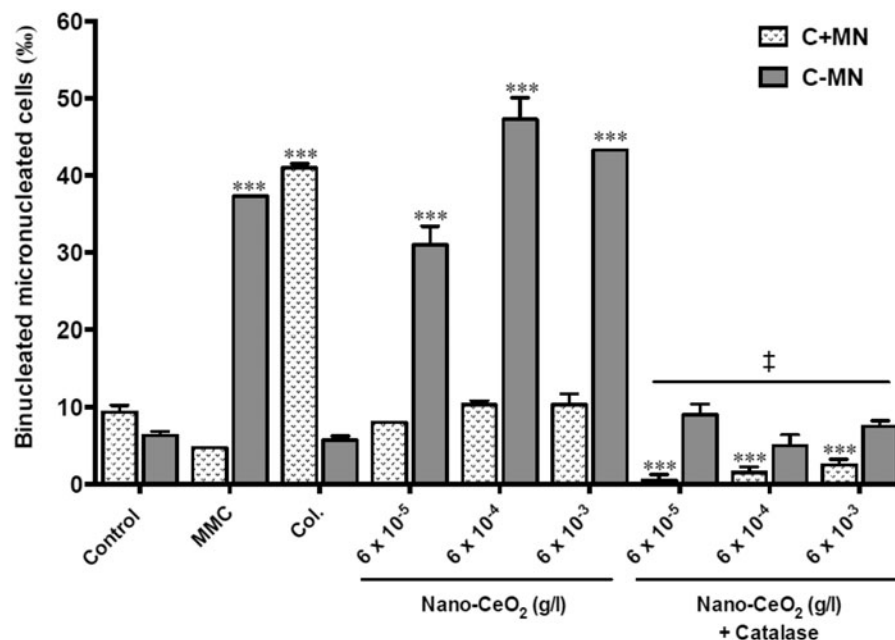


Figure 3. Frequency of centromere-positive (C+MN) and centromere negative (C-MN) micronuclei in binucleated human dermal fibroblasts incubated for 48 h with 10 ng/ml mitomycin C (MMC), 25 nM colchicine (Col.) or nano-CeO<sub>2</sub> ( $6 \times 10^{-5}$ – $6 \times 10^{-3}$  g/l; 0.22–22  $\mu$ M)  $\pm$  catalase (500 U/ml) assessed by the CBMN assay in combination with immunofluorescence staining of CENP-A. Data represent means  $\pm$  SEM of  $n = 3$  independent experiments made in duplicate. One-way ANOVA followed by Tukey test: \*\*\* $p < 0.001$  vs control cells (DMEM medium); † $p < 0.01$  versus cells treated with nano-CeO<sub>2</sub> alone at the same concentration.



To assess if MN formed upon exposure of fibroblasts to nano-CeO<sub>2</sub> is associated with clastogenic (C-MN) or aneugenic (C+MN) damages, CBMN assays in combination with CENP-A analysis were carried out under the conditions of Figure 2. Compared to control untreated cells, mitomycin C and colchicine yielded the expected responses, i.e. a significant increase in C-MN ( $p < 0.001$ ) and C+MN ( $p < 0.001$ ), respectively (Figure 3). At any tested concentration, cells exposed to nano-CeO<sub>2</sub> for 48 h showed a significant increase in C-MN ( $p < 0.001$  versus control) but not C+MN, which remained at the control level. This demonstrates a nano-CeO<sub>2</sub>-induced clastogenic mechanism of chromosomal damage, leading to structural chromosomal aberrations. In the presence of 500 U/ml catalase, this clastogenic effect of nano-CeO<sub>2</sub> was inhibited to the baseline level, suggesting the implication of H<sub>2</sub>O<sub>2</sub> (Figure 3).

#### Assessment of CeO<sub>2</sub> particles-induced lipid peroxidation

Spectrophotometric measurement of MDA-TBA levels was used to determine lipid peroxidation in fibroblasts incubated for 48 h in the presence of CeO<sub>2</sub> particles as described above. A baseline level of MDA-TBA was found in untreated cells, which was not affected by including catalase (500 U/ml) or the cell glutathione precursor NAC (2 mM). Upon addition of 0.5 mM H<sub>2</sub>O<sub>2</sub> for 48 h to the culture medium, MDA-TBA levels augmented as a result of increased cell lipid peroxidation (Figure 4A). A concomitant moderate cytotoxic effect was observed for H<sub>2</sub>O<sub>2</sub>-treated cells (~25% loss in viability versus control cells,  $p < 0.05$ , data not shown) by the viability MTT assay performed as described (Culcasi et al., 2012). In nano-CeO<sub>2</sub>-loaded cells, the elevation of MDA-TBA levels became significant when the particles dose was  $\geq 6 \times 10^{-4}$  g/l, peaking at ~3-times of the control value. A ~20% decrease in viability ( $p < 0.05$  versus control cells) was obtained for cells treated with  $6 \times 10^{-3}$  g/l (22  $\mu$ M) of nano-CeO<sub>2</sub> showing a low cytotoxicity at this concentration. As expected from their H<sub>2</sub>O<sub>2</sub> inhibiting properties NAC and, in a lesser extent, catalase significantly lowered this MDA-TBA formation ( $p < 0.01$  versus nano-CeO<sub>2</sub>-treated cells). Again, even when co-incubated at  $6 \times 10^{-3}$  g/l, micro-CeO<sub>2</sub> did not induce any significant cell lipid peroxidation (Figure 4A).

#### Intracellular GSH/GSSG ratio upon CeO<sub>2</sub> particles treatment

As a consequence of lipid peroxidation induced by 48 h exposure to CeO<sub>2</sub> particles seen in Figure 4(A), the GSH/GSSG ratio of treated cells was calculated, as a dynamic index of cell glutathione status. As expected, the baseline GSH/GSSG value ( $4.6 \pm 0.5 / 1.9 \pm 0.4$  nmol/mg prot.) was not affected by 500 U/ml catalase ( $4.0 \pm 0.1 / 2.1 \pm 0.2$  nmol/mg prot.) while it increased by ~3-times upon addition of 2 mM NAC ( $7.5 \pm 1.3 / 1.1 \pm 0.3$  nmol/mg prot.). The ratio significantly decreased upon treatment with  $6 \times 10^{-4}$  g/l nano-CeO<sub>2</sub> ( $p < 0.01$  versus control) and supplementation with NAC partially restored baseline levels (Figure 4B). Consistent with the lipid peroxidation data (Figure 4A), higher levels of GSH/GSSG were recovered either upon adding catalase to nano-CeO<sub>2</sub>-treated cells or by using micro-CeO<sub>2</sub> instead of nano-CeO<sub>2</sub> (Figure 4B). Taken together these data suggest a strong implication of H<sub>2</sub>O<sub>2</sub> formation in the modulation of GSH/GSSG ratio.

#### Modification of the oxidation state of nano-CeO<sub>2</sub> by ascorbate

Previously, we reported an extracellular release of ascorbate in cultured human fibroblasts shortly exposed to low-cytotoxic nano-CeO<sub>2</sub> (Culcasi et al., 2012). XANES measurements were performed at the Ce L<sub>3</sub>-edge to check for potential structural changes that would occur at the nano-CeO<sub>2</sub> surface following such ascorbate release. Thus, a 2:1 mixture of nano-CeO<sub>2</sub> (20 mM):ascorbate (10 mM) was incubated for 24 h in Milli-q water (pH 7.4) to saturate the surface of the particles. The shape of XANES spectra and the position of the edge are easily distinguishable for Ce<sup>3+</sup> and Ce<sup>4+</sup> reference compounds, i.e. one absorption edge for Ce<sup>3+</sup> and a doublet for Ce<sup>4+</sup> (Figure 5). Consequently, a slight change in the redox state (a reduction) of nano-CeO<sub>2</sub> during the interaction with ascorbate can be easily quantified through linear combination of Ce<sup>3+</sup> reference compounds (as CeCl<sub>3</sub>) and nano-CeO<sub>2</sub>. The results of the LCF (Figure 5) indicated that after 24 h incubation with ascorbate,  $17 \pm 2\%$  of the XANES signal of the nano-CeO<sub>2</sub> can be attributed to the signal of the Ce<sup>3+</sup> reference compound. Assuming that 35–40% of the Ce atoms are localized at the surface of the

Figure 4. Induction of oxidative stress in human fibroblasts after 48 h incubation in the presence of CeO<sub>2</sub> particles and inhibition by antioxidants. (A) Lipid peroxidation measured by the MDA-TBA assay. (B) Intracellular glutathione status measured by the GSH/GSSG ratio. Data represent means  $\pm$  SEM of  $n = 4$  independent experiments made in triplicate. One-way ANOVA followed by Tukey test: \* $p < 0.05$ ; \*\* $p < 0.01$  and \*\*\* $p < 0.001$  versus control cells (DMEM group); § $p < 0.01$  versus NAC-treated control cells (DMEM + NAC group); ‡ $p < 0.01$  versus cells treated with nano-CeO<sub>2</sub> alone at the same concentration. Cells incubated for 48 h in DMEM + 0.5 mM H<sub>2</sub>O<sub>2</sub> are used as a positive control. Concentrations used: catalase, 500 U/ml and NAC, 2 mM.

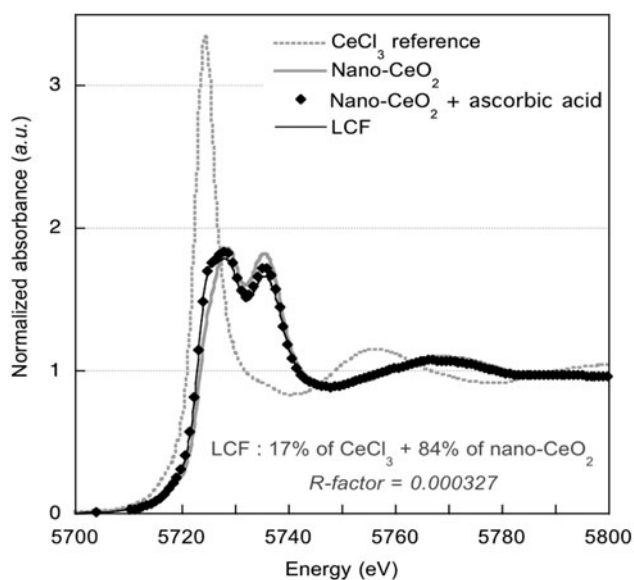
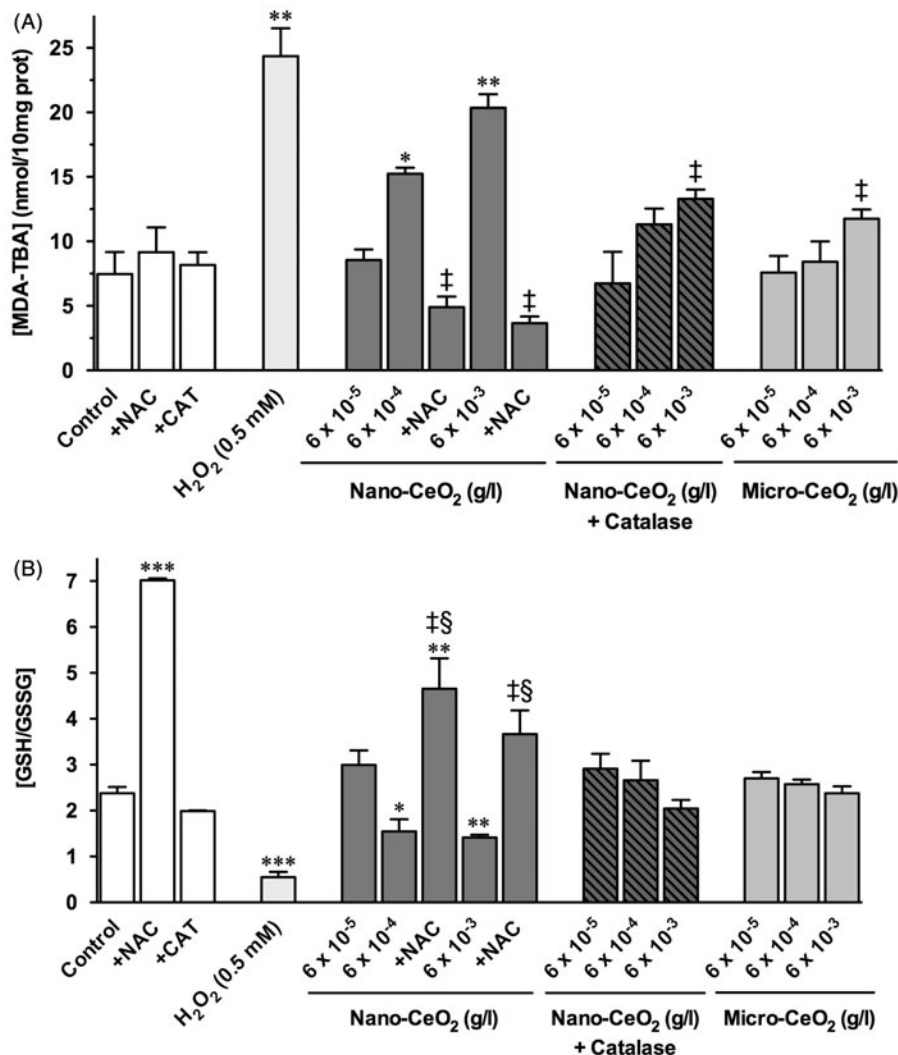


Figure 5. XANES at the Ce L<sub>3</sub>-edge of nano-CeO<sub>2</sub> before and after 24 h incubation with ascorbate. The experimental spectra are compared to the spectra of the initial nano-CeO<sub>2</sub> and of Ce(III) reference compound (as CeCl<sub>3</sub>). R-factor: residue of the fit. Fitting range: -9 to +36 eV above the edge. LCF: linear combination fit.

nano-CeO<sub>2</sub> (for a 7 nm-diameter sphere with a surface layer of 5 Å-thickness), this indicates that 42–48% of the Ce<sup>4+</sup> atoms of the surface were reduced into Ce<sup>3+</sup>.

## Discussion

This study investigates the mechanisms by which nano-CeO<sub>2</sub> induces genotoxicity to human dermal fibroblasts, using the CBMN assay. Importantly, the lowest nano-CeO<sub>2</sub> doses used in this study, relevant to chronic exposure situations (i.e.  $6 \times 10^{-5}$ – $6 \times 10^{-4}$  g/l; 0.22–2.2 μM), that significantly increased the MN frequency of treated cells did not induce significant cytotoxicity, i.e. loss of viability and necrosis (Culcasi et al., 2012). Although these doses are at least two orders of magnitude lower than those reported to induce mitochondrial damage and ROS formation, i.e. above  $10^{-3}$  g/l (Culcasi et al., 2012; Karlsson et al., 2009), we postulated that they may induce the release of small amounts of oxygen-derived free radicals as an early signaling mechanism through protein synthesis and membrane NADPH oxidase stimulation (Culcasi et al., 2012).

In the present study, MN analysis evidenced for the first time a nano-CeO<sub>2</sub>-induced significant increase in the centromere-negative MN relative to untreated cells (Figure 2). These results clearly demonstrate a chromosomal endpoint of nano-CeO<sub>2</sub> genotoxicity, expressed as a clastogenic effect, which is related

to acentric chromosomal fragments formed by unrepaired double-strand breaks or by misrepair of various DNA lesions. The MN frequency consecutive to DNA damage induced by clastogenic events plays a role in the early stages of human carcinogenesis (Bonassi et al., 2007).

About one-hundred studies have addressed the genotoxicity induced by engineered nanoparticles, but in most of them the comet assay was predominantly used (reviewed in Magdolenova et al., 2014). By this technique, Auffan et al., (2009b) and De Marzi et al., (2013) demonstrated genotoxicity of nanoceria in different cell lines while no effects were found in human lens epithelial cells (Pierscionek et al., 2010). In contrast, the MN methodology was applied in few studies to better explore the mechanisms underlying the primary direct genotoxic effects in a variety of systems, including ultrafine TiO<sub>2</sub> in Syrian hamster embryo fibroblasts (Rahman et al., 2002), silica nanoparticles in human A549 cells (Gonzalez et al., 2010), gold nanoparticles in human lymphocytes and murine macrophages (Di Bucchianico et al., 2014), multi-wall carbon nanotubes in AT-II pneumocytes, human MCF-7 fibroblasts and rat epithelial cells (Muller et al., 2008), and nanoparticles from a cobalt-chromium alloy in human MCF-7 fibroblasts (Papageorgiou et al., 2007). Using the MN methodology, we found herein a clastogenic effect (chromosomal break) to be likely responsible for the genotoxicity of nano-CeO<sub>2</sub>, consistent with an earlier study on other insoluble oxide nanoparticles (Rahman et al., 2002). Of interest, all non-oxide nanomaterials previously studied showed aneugenic-based genotoxic mechanisms leading to chromosome instability (Di Bucchianico et al., 2014; Muller et al., 2008; Papageorgiou et al., 2007).

Compared to the nanosized material, micro-CeO<sub>2</sub> showed significantly lower genotoxic properties (Figure 2A), possibly related to the tenfold higher SSA of these particles (Auffan et al., 2009b; Spalla & Cabane, 1993; Thill et al., 2006), which can diminish their surface reactivity with cellular components. Karlsson et al. (2009) reported both decreased cytotoxicity and genotoxicity of CuO micro-particles on the human cell line A549, which was attributed to their less marked ability to damage the mitochondria. However, perusal of literature data shows that, for several oxide nanomaterials (e.g. TiO<sub>2</sub>, Fe<sub>3</sub>O<sub>4</sub> and Fe<sub>2</sub>O<sub>3</sub>), such a decrease of toxicity with increase of particles size is not a general feature (Karlsson et al., 2009; Guichard et al., 2012). Clearly, this enhanced genotoxicity of nano- versus micro-CeO<sub>2</sub> cannot be explained by differences in zeta potentials, i.e. in a better ability of the nanoparticles to penetrate cells due to a more negative charge (Patil et al., 2007). In this study, we have evidenced other physical parameters that may be account for the enhanced genotoxicity of nano-CeO<sub>2</sub>, such as differences in their agglomeration process in DMEM and the size of the resulting aggregates (Figure 1). In this regard, it was recently proposed that particles under 50 nm size (including nanoceria) can only be uptaken by cells as agglomerates. Therefore, the degree of agglomeration could be a dominant factor in the cellular uptake, vesiculation, diffusion and/or sedimentation of particles leading to significant differences in toxicity (Limbach et al., 2005).

Recently, we reported that a key mechanism of nano-CeO<sub>2</sub> cytotoxicity in human fibroblasts was linked to the ability of the particles to stimulate the mitochondrial sources of ROS, in particular O<sub>2</sub><sup>-</sup> and H<sub>2</sub>O<sub>2</sub>. In these cells, nano-CeO<sub>2</sub>-induced formation of ROS provoked a significant decrease in mitochondrial membrane potential and apoptosis at millimolar concentrations that caused loss of cell viability (Culcasi et al., 2012). In this context of induction of ROS formation by nanoparticles, the reported mitochondria-related, genotoxic effect of CuO nanoparticles (Karlsson et al., 2009) could be attributed to the known Fenton-like properties of Cu<sup>2+</sup> in the presence of H<sub>2</sub>O<sub>2</sub> (Valko et al., 2006). However, the pertinence of the Fenton reaction as a

privileged trigger of ROS formation in cells was ruled out since nanoparticles from very potent Fenton catalysts such as Fe<sup>2+</sup>/Fe<sup>3+</sup> did not induce increased genotoxicity compared to CuO nanoparticles (Karlsson et al., 2009). Using ESR spin trapping, we have found that Ce<sup>3+</sup>/Ce<sup>4+</sup> and nanoceria are not good catalysts for HO<sup>•</sup> formation from H<sub>2</sub>O<sub>2</sub> (Culcasi et al., 2012). As a mechanism of mitochondrial damage, it has been proposed that nanoparticles at the millimolar range can interact physically with mitochondrial membranes and the permeability transition pore, enhancing ROS production and cell death (Karlsson et al., 2009 and references therein). Here, at non cytotoxic, micromolar levels, inhibition of nano-CeO<sub>2</sub> genotoxicity with catalase (Figures 2 and 3) supports our previous finding that, under these conditions, NADPH oxidase may be stimulated to release O<sub>2</sub><sup>-</sup>/H<sub>2</sub>O<sub>2</sub> by activation of Nox2 and Nox4 complexes (Culcasi et al., 2012).

In general, DNA damage and oxidative DNA lesions are associated with ROS formation and cell diffusion, the release of toxic ions from particles and/or direct physical interaction with chromosomes (recently Magdolenova et al. (2014) provided the illustration of different routes by which nanoparticles induced genotoxicity by indirect or direct DNA binding). To our knowledge, this latter possibility appears unlikely in the particular case of the nano-CeO<sub>2</sub> used in the present study because TEM studies have shown that the aggregates of these nanoceria are rapidly adsorbed onto the external cell membrane and internalized within the cytoplasm and large vesicles, without significantly reaching the mitochondria and the nucleus (Auffan et al., 2009b). Indeed, there is a large discrepancy within the sub-cellular distribution data for nanoceria, probably due to the intrinsic differences in nanoceria preparation and/or properties such as the size of agglomerates in different media, or the multiplicity of cells that are used in the literature. Some studies have failed to localize the particles aggregates in the nucleus (Hussain et al., 2012; Karlsson et al., 2009; Nel et al., 2006) while the rapid uptake (within 3 h) and distribution of nanoceria conjugated to a fluorescent probe in the mitochondria and nucleus was clearly demonstrated (Singh et al., 2010). Interestingly in this latter study, despite average sizes of nanoceria were of ~50 nm, no aggregation of the well-dispersed material occurred when cells were incubated for 3 h in phosphate saline buffer (Singh et al., 2010). In general, well-dispersed nanoparticles were found less cytotoxic than agglomerates (Magdolenova et al., 2014 and references therein).

Consequently, under the experimental conditions of our study where we can assume that agglomerated nano-CeO<sub>2</sub> are uptaken by the cells, one likely mechanism of nano-CeO<sub>2</sub> clastogenic effect would involve the diffusion of O<sub>2</sub><sup>-</sup>/H<sub>2</sub>O<sub>2</sub> (formed in the mitochondria and/or when membrane NADPH oxidase is stimulated) to the nucleus where it can undergo metal-catalyzed conversion into the harmful HO<sup>•</sup> to react with DNA (Halliwell & Aruoma, 1991). In support to this diffusion-based mechanism were the findings that added catalase, which cannot reach the nucleus, decreased the MN (Figure 2A) and C-MN and C + MN (Figure 3) levels. Reductions of MN levels in different mammalian cells challenged with magnetite nanoparticles were observed by Könczöl et al. (2011) and Kawanishi et al. (2013) upon treatment with the antioxidants butylated hydroxyanisole, α-tocopherol or NAC.

Another possible origin of nano-CeO<sub>2</sub> genotoxicity would involve subtle mechanical deformations of the nucleus by large intracellular vesicles of aggregates, which may disturb mitosis without any contact with DNA (Magdolenova et al. (2014) and reference therein).

Obviously, DNA was not the only target of nano-CeO<sub>2</sub>-induced ROS production and cells exposed to the particles showed parallel indices of lipid peroxidation and GSH/GSSG ratio decrease (Figure 4). Previous studies have documented the depletion of the

antioxidant pool (GSH,  $\alpha$ -tocopherol) or induction of oxidative-stress related genes (heme oxygenase-1) in cells exposed to nanoceria (Eom & Choi, 2009; Lin et al., 2006; Park et al., 2008). Zhao et al. (2012) reported that nano-CeO<sub>2</sub> caused stress response in corn plants by over cell production, accumulation of H<sub>2</sub>O<sub>2</sub> and up-regulation of heat shock protein. Here, we observed that the effect of nano-CeO<sub>2</sub> on GSH/GSSG was also reversed by NAC (Figure 4) suggesting that the cooperation between GSH and the mitochondrial enzyme glutathion peroxidase is strongly involved in cell protection against the nanoparticles. A third indirect source of nano-CeO<sub>2</sub> genotoxicity could be MDA formation (Figure 4A), a proven mutagen and carcinogenic compound which react with DNA (Valko et al., 2006).

A recognized detrimental effect of ascorbate in biological systems is related to its reductant role to shift poorly catalytic metals into highly effective catalyzers (e.g. Fe<sup>3+</sup> → Fe<sup>2+</sup>) that would promote formation of HO<sup>•</sup> via the Fenton reaction. Previously, we detected by ESR an extracellular release of ascorbate in fibroblasts incubated with nano-CeO<sub>2</sub> at doses as low as 10<sup>-6</sup> g/l (Culcasi et al., 2012), making this event relevant to the conditions of the present study. In this study, *in vitro* XANES analysis evidenced a surface interaction of ascorbate with nano-CeO<sub>2</sub>, leading to a significant shift of the Ce<sup>4+</sup>/Ce<sup>3+</sup> redox cycle toward the reduced cerous form (Figure 5). The extent to which such a structural change is biologically relevant and may have implications in the genotoxic effect of nano-CeO<sub>2</sub> needs to be determined. Of interest, however (i) raising the Ce<sup>3+</sup> proportion at the surface of nano-CeO<sub>2</sub> increased DNA damage and lipid peroxidation (Kuchma et al., 2010), and (ii) incubating or administrating Ce<sup>3+</sup> as free ion to cells or animals resulted in protein damage, including hemoglobin, heme-Fe(II) or superoxide dismutase (Cheng et al., 2000; Liu et al., 2008).

## Conclusions

CBMN assay and centromere analysis revealed a significant increase in centromere-negative MN of cells exposed with nano-CeO<sub>2</sub> but not micro-CeO<sub>2</sub>. These results clearly demonstrate a chromosomal endpoint of genotoxicity for nano-CeO<sub>2</sub>, expressed as a clastogenic effect, consistent with cellular ROS production which is considered as an important endogenous source of DNA damage and mutations contributing to human genetic disease. At concentrations above 6 x 10<sup>-5</sup> M, nano-CeO<sub>2</sub> also induced lipid peroxidation and decline of cellular glutathione level. ROS and by-products of lipid peroxidation such as MDA are likely to play a major role in producing the genotoxic effects in terms of clastogenic damage. Inhibition of both genotoxic effect and oxidative stress by catalase and NAC suggest that control of H<sub>2</sub>O<sub>2</sub> levels is a key factor of cell protection. Altogether our data strengthen the need for a better clinical evaluation of nano-CeO<sub>2</sub> genotoxic effects.

## Acknowledgements

The authors thank J. Pompili for her excellent technical assistance, the ELETTRA synchrotron staff in Trieste (Italy) for providing XAFS 11.1 beam time and local contacts for their help during the experiment. The authors thank Drs B Courbière and T Orsière for giving access to the cell culture platform.

## Declaration of interest

The authors declare that they have no conflict of interest. The authors gratefully acknowledge the CNRS for funding the iCEINT International Consortium for the Environmental Implications of Nanotechnology. Additional financial supports were provided by the Post-Grenelle (French Ministry of Ecology and Sustainable Development) via the Antiopes (INERIS) network (IMPECNANO project). MCA acknowledges the SARL YELEN (Ensuès-la-Redonne, France) for financial support.

## References

- Albertini RJ, Anderson D, Douglas GR, Hagmar L, Hemminki K, Merlo F, et al. 2000. IPCS guidelines for the monitoring of genotoxic effects of carcinogens in humans. *Mutat Res* 463:111–72.
- Asati A, Santra S, Kaittanis C, Nath S, Perez JM. 2009. Oxidase-like activity of polymer-coated cerium oxide nanoparticles. *Angew Chem Int Ed* 48:2308–12.
- Auffan M, Rose J, Bottero JY, Lowry GV, Jolivet JP, Wiesner MR. 2009a. Towards a definition of inorganic nanoparticles from an environmental, health and safety perspective. *Nat Nanotechnol* 4:634–41.
- Auffan M, Rose J, Orsière T, De Meo M, Thill A, Zeyons O, et al. 2009b. CeO<sub>2</sub> nanoparticles induce DNA damage towards human dermal fibroblasts *in vitro*. *Nanotoxicology* 3:161–71.
- Benameur L, Orsière T, Rose J, Botta A. 2011. Detection of environmental clastogens and aneugens in human fibroblasts by cytokinesis-blocked micronucleus assay associated with immunofluorescent staining of CENP-A in micronuclei. *Chemosphere* 84:676–80.
- Bonassi S, Znaor A, Ceppi M, Lando C, Chang WP, Holland N, et al. 2007. An increased micronucleus frequency in peripheral blood lymphocytes predicts the risk of cancer in humans. *Carcinogenesis* 28:625–31.
- Campbell CT, Peden CH. 2005. Chemistry: oxygen vacancies and catalysis on ceria surfaces. *Science* 309:713–14.
- Cheng G, Guo W, Hana L, Chen E, Kong L, Wang L, et al. 2013. Cerium oxide nanoparticles induce cytotoxicity in human hepatoma SMMC-7721 cells via oxidative stress and the activation of MAPK signaling pathways. *Toxicol In Vitro* 27:1082–8.
- Cheng Y, Li Y, Li R, Lu J, Wang K. 2000. Orally administrated cerium chloride induces the conformational changes of rat hemoglobin, the hydrolysis of 2,3-DPG and the oxidation of heme-Fe(II), leading to changes of oxygen affinity. *Chem Biol Interact* 125:191–208.
- Cho WS, Duffin R, Poland CA, Howie SEM, MacNee W, Bradley M, et al. 2010. Metal oxide nanoparticles induce unique inflammatory footprints in the lung: important implications for nanoparticle testing. *Environ Health Persp* 118:1699–706.
- Culcasi M, Benameur L, Mercier A, Lucchesi C, Rahmouni H, Asteian A, et al. 2012. EPR spin trapping evaluation of ROS production in human fibroblasts exposed to cerium oxide nanoparticles: evidence for NADPH oxidase and mitochondrial stimulation. *Chem Biol Interact* 199:161–76.
- Culcasi M, Muller A, Mercier A, Clément JL, Payet O, Rockenbauer A, et al. 2006. Early specific free radical-related cytotoxicity of gas phase cigarette smoke and its paradoxical temporary inhibition by tar: an electron paramagnetic resonance study with the spin trap DEPMPO. *Chem Biol Interact* 164:215–31.
- De Faria LA, Trasatti S. 1994. The point of zero charge of CeO<sub>2</sub>. *J Colloid Interface Sci* 167:352–7.
- De Marzi L, Monaco A, De Lapuente J, Ramos D, Borrás M, Di Gioacchino M, et al. 2013. Cytotoxicity and genotoxicity of ceria nanoparticles on different cell lines *in vitro*. *Int J Mol Sci* 14:3065–77.
- Di Bucchianico S, Fabbrizi MR, Cirillo S, Ubaldi C, Gilliland D, Valsami-Jones E, Migliore L. 2014. Aneuploidogenic effects and DNA oxidation induced *in vitro* by differently sized gold nanoparticles. *Int J Nanomedicine* 9:2191–204.
- Di Cicco A, Aquilanti G, Minicucci M, Principi E, Novello N, Cognigni A, Olivi L. 2009. Novel XAFS capabilities at ELETTRA synchrotron light source. *J Phys Conf Ser* 190:012043.
- Esch F, Fabris S, Zhou L, Montini T, Africh C, Fornasiero P, et al. 2005. Electron localization determines defect formation on ceria substrates. *Science* 309:752–5.
- Eom H, Choi J. 2009. Oxidative stress of CeO<sub>2</sub> nanoparticles via p38-Nrf-2 signaling pathway in human bronchial epithelial cell, Beas-2B. *Toxicol Lett* 187:77–83.
- Fenech M. 2007. Cytokinesis-block micronucleus cytome assay. *Nat Protoc* 2:1084–104.
- Gonzalez L, Thomassen LC, Plas G, Rabolli V, Napierska D, Decordier I, et al. 2010. Exploring the aneugenic and clastogenic potential in the nanosize range: A549 human lung carcinoma cells and amorphous monodisperse silica nanoparticles as models. *Nanotoxicology* 4:82–95.
- Guichard Y, Schmit J, Darne C, Gaté L, Goutet M, Rousset D, et al. 2012. Cytotoxicity and genotoxicity of nanosized and microsized titanium oxide and iron oxide particles in Syrian hamster embryo cells. *Ann Occup Hyg* 56:631–44.

- Halliwell B, Aruoma OI. 1991. DNA damage by oxygen-derived species. Its mechanism and measurement in mammalian systems. *FEBS Lett* 281:9–19.
- Hussain S, Al-Nsour F, Rice AB, Marshburn J, Ji B, Zink JJ, et al. 2012. Cerium dioxide nanoparticles induce apoptosis and autophagy in human peripheral blood monocytes. *ACS Nano* 6:5820–9.
- Izu N, Shin W, Matsubara I, Murayama N. 2004. Development of resistive oxygen sensors based on cerium oxide thick film. *J Electroceramics* 13: 703–6.
- Jasinski P, Suzuki T, Anderson HU. 2003. Nanocrystalline undoped ceria oxygen sensor. *Sens Actuators B* 95:73–7.
- Karlsson HL, Cronholm P, Gustafsson J, Moller L. 2008. Copper oxide nanoparticles are highly toxic: a comparison between metal oxide nanoparticles and carbon nanotubes. *Chem Res Toxicol* 21:1726–32.
- Karlsson HL, Gustafsson J, Cronholm P, Moller L. 2009. Size-dependent toxicity of metal oxide particles: a comparison between nano- and micrometer size. *Toxicol Lett* 188:112–18.
- Katschinsky DM, Boos K, Schindler SG, Fandrey J. 2000. Pivotal role of reactive oxygen species as intracellular mediators of hyperthermia-induced apoptosis. *J Biol Chem* 275:21094–8.
- Kawanishi M, Ogo S, Ikemoto M, Totsuka Y, Ishino K, Wakabayashi K, Yagi T. 2013. Genotoxicity and reactive oxygen species production induced by magnetite nanoparticles in mammalian cells. *J Toxicol Sci* 38:503–11.
- Kirsch-Volders M, Vanhauwaert A, De Boeck M, Decordier I. 2002. Importance of detecting numerical versus structural chromosome aberrations. *Mutat Res* 504:137–48.
- Kirsch-Volders M, Sofuni T, Aardema M, Albertini S, Eastmond D, Fenech M, et al. 2003. Report from the *in vitro* micronucleus assay working group. *Mutat Res* 540:153–63.
- Könczöl M, Ebeling S, Goldenberg E, Treude F, Gminski R, Gieré R, et al. 2011. Cytotoxicity and genotoxicity of size-fractionated iron oxide (magnetite) in A549 human lung epithelial cells: role of ROS, JNK, and NF- $\kappa$ B. *Chem Res Toxicol* 24:1460–75.
- Kuchma MH, Komanski CB, Colon J, Teblum A, Masunov AE, Alvarado B, et al. 2010. Phosphate ester hydrolysis of biologically relevant molecules by cerium oxide nanoparticles. *Nanomedicine* 6: 738–44.
- Li Y, Dong X, Gao J, Hei D, Zhou X, Zhang H. 2009. A highly sensitive g-radiation dosimeter based on the CeO<sub>2</sub> nanowires. *Physica E* 4: 1550–3.
- Limbach LK, Li Y, Grass RN, Brunner TJ, Hintermann MA, Muller M, et al. 2005. Oxide nanoparticle uptake in human lung fibroblasts: effects of particle size, agglomeration, and diffusion at low concentration. *Environ Sci Technol* 39:9370–6.
- Lin W, Huang YW, Zhou XD, Ma Y. 2006. Toxicity of cerium oxide nanoparticles in human lung cancer cells. *Int J Toxicol* 25:451–7.
- Liu P, Ma L, Yin S, Hong F. 2008. Effect of Ce<sup>3+</sup> on conformation and activity of superoxide dismutase. *Biol Trace Elem Res* 125:170–8.
- Long T, Saleh N, Tilton R, Lowry GV, Veronesi B. 2006. Titanium dioxide (P25) produces oxidative stress in immortalized brain microglia (BV2): implication of nanoparticle neurotoxicity. *Environ Sci Technol* 40:4346–52.
- Lowry OH, Rosebrough NJ, Farr AL, Randall RJ. 1951. Protein measurement with the Folin phenol reagent. *J Biol Chem* 193:265–75.
- Ma JY, Mercer R, Barger M, Schwegler-Berry D, Scabillon J, Ma JK, Castranova V. 2012. Induction of pulmonary fibrosis by cerium oxide nanoparticles. *Toxicol Appl Pharm* 262:255–64.
- Magdolenova Z, Collins A, Kumar A, Dhawan A, Stone V, Dusinska M. 2014. Mechanisms of genotoxicity. A review of *in vitro* and *in vivo* studies with engineered nanoparticles. *Nanotoxicology* 8:233–78.
- Mateuca R, Lombaert N, Aka PV, Decordier I, Kirsch-Volders M. 2006. Chromosomal changes: induction, detection methods and applicability in human biomonitoring. *Biochimie (Paris)* 88:1515–31.
- Meitzner G, Gardea-Torresdey J, Parsons J, Scott SL, Deguns EW. 2005. The effect of cryogenic sample cooling on X-ray absorption spectra. *Microchem J* 81:61–8.
- Muller J, Decordier I, Hoet PH, Lombaert N, Thomassen L, Huaux F, et al. 2008. Clastogenic and aneuploidic effects of multi-wall carbon nanotubes in epithelial cells. *Carcinogenesis* 29:427–33.
- Nabavi M, Spalla O, Cabane B. 1993. Surface chemistry of nanometric ceria particles in aqueous dispersion. *J Colloid Interface Sci* 160: 459–71.
- Nahm WK, Zhou L, Falanga V. 2002. Sustained ability for fibroblast outgrowth from stored neonatal foreskin: a model for studying mechanisms of fibroblast outgrowth. *J Dermatol Sci* 28:152–8.
- Nel A, Xia T, Mädler L, Li N. 2006. Toxic potential of materials at the nanolevel. *Science* 311:622–7.
- Newville M. 2001. IFEFFIT: interactive XAFS analysis and FEFF fitting. *J Synchrotron Radiat* 8:322–4.
- Papageorgiou I, Brown C, Schins R, Singh S, Newson R, Davis S, et al. 2007. The effect of nano- and micron-sized particles of cobalt–chromium alloy on human fibroblasts *in vitro*. *Biomaterials* 28: 2946–58.
- Park B, Martin P, Harris C, Guest R, Whittingham A, Jenkinson P, Handley J. 2007. Initial *in vitro* screening approach to investigate the potential health and environmental hazards of Envirox™ – a nanoparticulate cerium oxide diesel fuel additive. *Part Fibre Toxicol* 4:12.
- Park EJ, Choi J, Park YK, Park K. 2008. Oxidative stress induced by cerium oxide nanoparticles in cultured BEAS-2B cells. *Toxicology* 245:90–100.
- Patil S, Kuiry SC, Seal S, Vanfleet R. 2002. Synthesis of nanocrystalline ceria particles for high temperature oxidation resistant coating. *J Nanoparticle Res* 4:433–8.
- Patil S, Sandberg A, Heckert E, Self W, Seal S. 2007. Protein adsorption and cellular uptake of cerium oxide nanoparticles as a function of zeta potential. *Biomaterials* 28:4600–7.
- Pierscionek BK, Li Y, Yasseen AA, Colhoun LM, Schachar RA, Chen W. 2010. Nanoceria have no genotoxic effect on human lens epithelial cells. *Nanotechnology* 21:035102.
- Rahman Q, Lohani M, Dopp E, Pemsel H, Jonas L, Weiss DG, Schiffmann D. 2002. Evidence that ultrafine titanium dioxide induces micronuclei and apoptosis in syrian hamster embryo fibroblasts. *Environ Health Persp* 110:797–800.
- Rogers NJ, Franklin NM, Apte SC, Batley GE, Angel BM, Lead JR, Baalousha M. 2010. Physico-chemical behaviour and algal toxicity of nanoparticulate CeO<sub>2</sub> in freshwater. *Environ Chem* 7:50–60.
- Sayes CM, Gobin AM, Ausman KD, Mendez J, West JL, Colvin VL. 2005. Nano-C<sub>60</sub> cytotoxicity is due to lipid peroxidation. *Biomaterials* 26:7587–95.
- Sharma CS, Sarkar S, Periyakaruppan A, Barr J, Wise K, Thomas R, et al. 2007. Single-walled carbon nanotubes induces oxidative stress in rat lung epithelial cells. *J Nanosci Nanotechnol* 7:2466–72.
- Singh N, Manshian B, Jenkins GJ, Griffiths SM, Williams PM, Maffei TG, et al. 2009. Nanogenotoxicology: the DNA damaging potential of engineered nanomaterials. *Biomaterials* 30:3891–914.
- Singh S, Kumar A, Karakoti A, Seal S, Self WT. 2010. Unveiling the mechanism of uptake and sub-cellular distribution of cerium oxide nanoparticles. *Mol Biosyst* 6:1813–20.
- Spalla O, Cabane B. 1993. Growth of colloidal aggregates through polymer bridging. *Colloid Polym Sci* 271:357–71.
- Stern, ST, McNeil, SE. 2008. Nanotechnology safety concerns revisited. *Toxicol Sci* 101:4–21.
- Thill A, Zeyons O, Spalla O, Chauvat F, Rose J, Auffan M, Flank AM. 2006. Cytotoxicity of CeO<sub>2</sub> nanoparticles for *Escherichia coli*. Physico-chemical insight of the cytotoxicity mechanism. *Environ Sci Technol* 40:6151–6.
- Valko M, Rhodes CJ, Moncol J, Izakovic M, Mazur M. 2006. Free radicals, metals and antioxidants in oxidative stress-induced cancer. *Chem Biol Interact* 160:1–40.
- Wiesner MR, Lowry GV, Alvarez P, Dionysiou D, Biswas P. 2006. Assessing the risks of manufactured nanomaterials. *Environ Sci Technol* 40:4336–45.
- Zhao L, Peng B, Hernandez-Viezcás JA, Rico C, Sun Y, Peralta-Videa JR, et al. 2012. Stress response and tolerance of *Zea mays* to CeO<sub>2</sub> nanoparticles: cross talk among H<sub>2</sub>O<sub>2</sub>, heat shock protein, and lipid peroxidation. *ACS Nano* 6:9615–22.
- Zhang H, He X, Zhang Z, Zhang P, Li Y, Ma Y, et al. 2011. Nano-CeO<sub>2</sub> exhibits adverse effects at environmental relevant concentrations. *Environ Sci Technol* 45:3725–30.

Supplementary material available online

Supplementary Figure 6–8

## Supplementary Material

### DNA damage and oxidative stress induced by CeO<sub>2</sub> nanoparticles in human dermal fibroblasts: evidence of a clastogenic effect as a mechanism of genotoxicity

Laila Benameur<sup>1,2\*</sup>, Mélanie Auffan<sup>3,4</sup>, Mathieu Cassien<sup>1</sup>, Wei Liu<sup>2,3</sup>, Marcel Culcasi<sup>1</sup>, Hidayat Rahmouni<sup>1</sup>, Pierre Stocker<sup>1</sup>, Virginie Tassistro<sup>2</sup>, Jean-Yves Bottero<sup>3,4</sup>, Jérôme Rose<sup>3,4</sup>, Alain Botta<sup>2,4</sup>, Sylvia Pietri<sup>1</sup>

<sup>1</sup> Aix Marseille Université, CNRS, ICR UMR 7273, 13397, Marseille, France

<sup>2</sup> Aix-Marseille Université, CNRS, IMBE UMR 7263, 13385, Marseille, France

<sup>3</sup> Aix-Marseille Université, CNRS, CEREGE UMR 7330, 13545, Aix-en-Provence, France

<sup>4</sup> International Consortium for the Environmental Implications of Nanotechnology iCEINT, 13545, Aix-en-Provence, France

\* Corresponding author: Laila Benameur [laila.benameur@gmail.com](mailto:laila.benameur@gmail.com)

#### Supplementary 1. Structural characterization of nano-CeO<sub>2</sub> and micro-CeO<sub>2</sub>.

X-ray-absorption near-edge structure (XANES) spectroscopy at the Ce L<sub>3</sub>-edge was used to determine the local atomic geometry and the cerium oxidation state (Bianconi et al., 1987) of the nano-CeO<sub>2</sub> and micro-CeO<sub>2</sub> particles suspended for 1 h in abiotic DMEM, with aqueous CeCl<sub>3</sub> taken as reference for Ce(III). The XANES spectrum of CeCl<sub>3</sub> shows a single absorption jump or white line (5724 eV) corresponding to the 2p<sub>3/2</sub> → 4f<sup>1</sup>5d electronic transition (Takahashi et al., 2002), while those of CeO<sub>2</sub> crystallites exhibit a double white line with one peak (at 5728 eV) and a second peak (at 5735 eV) corresponding to the final state 2p4f<sup>1</sup>5d<sup>1</sup>L and 2p4f<sup>0</sup>5d<sup>2</sup> of Ce(IV) compounds,

respectively (Dexpert et al., 1987; Finkelstein et al., 1992) (Figure 6). These features of Figure 6 confirm the cerianite ( $\text{CeO}_2$ ) crystal structure for both nano- $\text{CeO}_2$  and micro- $\text{CeO}_2$ . This was also corroborated by X-ray diffraction for nano- $\text{CeO}_2$  (see supporting information in Auffan et al. 2009). The position of the main diffraction peaks at  $32.9^\circ$ ,  $55.4^\circ$  and  $66.2^\circ$  (Co  $K\alpha$ ) are in agreement with the crystallographic  $d$ -spacing of a cerianite reference standard, indicating that other crystalline species, if any, would account for less than 2–5% by weight (Auffan et al. 2009).

For both nano- $\text{CeO}_2$  and micro- $\text{CeO}_2$ , we did not notice any detectable peak at the absorption energy of Ce(III) on the XANES spectra. Since it can be estimated that the sensitivity of XANES to modification of the cerium oxidation state is around 8–10%, less than 10% of the Ce atoms in the abiotic DMEM medium would have been reduced to  $\text{Ce}^{3+}$ , leading to a non detectable increase of the corresponding Ce(III) XANES peak intensity. It was previously found that after a prolonged 24 h-incubation in abiotic DMEM or in presence of fibroblasts cells, a comparable 8–10% contribution of  $\text{Ce}^{3+}$  atoms at the surface of the particles was measured in the nano- $\text{CeO}_2$  solution (Auffan et al. 2009).

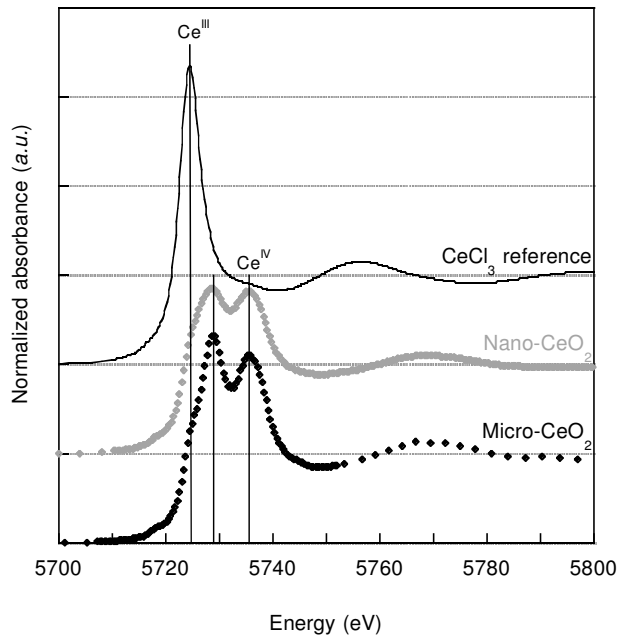


Figure 6: XANES spectroscopy at the Ce L<sub>3</sub>-edge of the nano-CeO<sub>2</sub> and micro-CeO<sub>2</sub> particles. The experimental spectra are obtained after 1 h incubation of the particles in DMEM and compared to the signal of CeCl<sub>3</sub>.

**Supplementary 2.** Surface charge measurements and agglomeration of particles as a function of pH and medium.

Zeta potentials of particles in water and DMEM were determined as described earlier (Nabavi et al. 1993; De Faria and Trasatti 1994). For nano-CeO<sub>2</sub> particles zeta potential data at physiological pH 6–7.3 and in alkaline water (point of zero charge, PZC) were published earlier in the literature (Nabavi et al. 1993; De Faria and Trasatti 1994, Thill et al. 2006 and references therein).

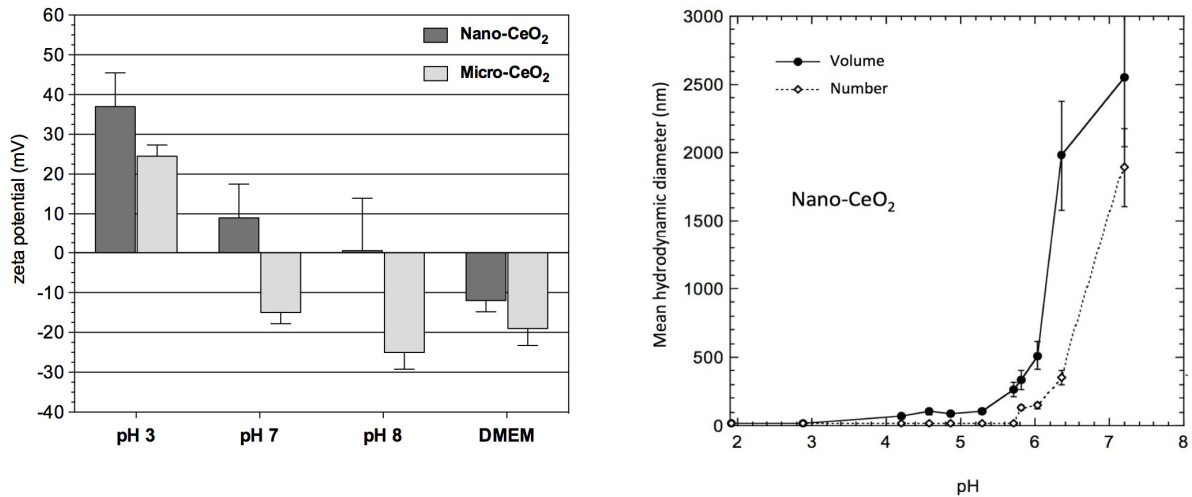


Figure 7: (left) Variation of the average hydrodynamic diameter of nano-CeO<sub>2</sub> as a function of pH in 10<sup>-3</sup> mol/l of NaCl. (right) Variation of the zeta potential of micro-CeO<sub>2</sub> and nano-CeO<sub>2</sub> particles as a function of pH (in water) and in culture medium (DMEM, pH 7.35).

### Supplementary 3. Micronucleus analysis of fibroblasts showing binucleated cells.

Micronuclei are an indicator of nuclear abnormalities such as chromosome breakage and/or whole chromosome loss. In order to distinguish between micronuclei formed in binucleated cells originating from a lagging acentric chromosome fragment (chromosome fragmentation, clastogenic mode of action) or from a lagging whole chromosome (aneugenic mode of action), the genotoxic mechanisms of nano-CeO<sub>2</sub> were determined using the cytokinesis-blocked micronucleus assay associated with immunofluorescence staining of centromere protein A in micronuclei. Figure 8 shows micronuclei formed in binucleated human dermal fibroblasts incubated for 48 h in several conditions. Nuclei and micronuclei stained with DAPI appear in blue. Centromeres were stained with CENP-A antibodies and then revealed by cyanine 3-conjugated secondary antibody (Cy3, red fluorescence). The red spots of fluorescence in the micronuclei of the binucleated

cells indicate the presence of whole chromosome and represent an aneugenic event (centromere positive, C+MN). However, those micronuclei that are centromere negative (C-MN) are a consequence of a clastogenic mode of action as they contain chromosome breaks (Figure 8A, 8C and 8D).

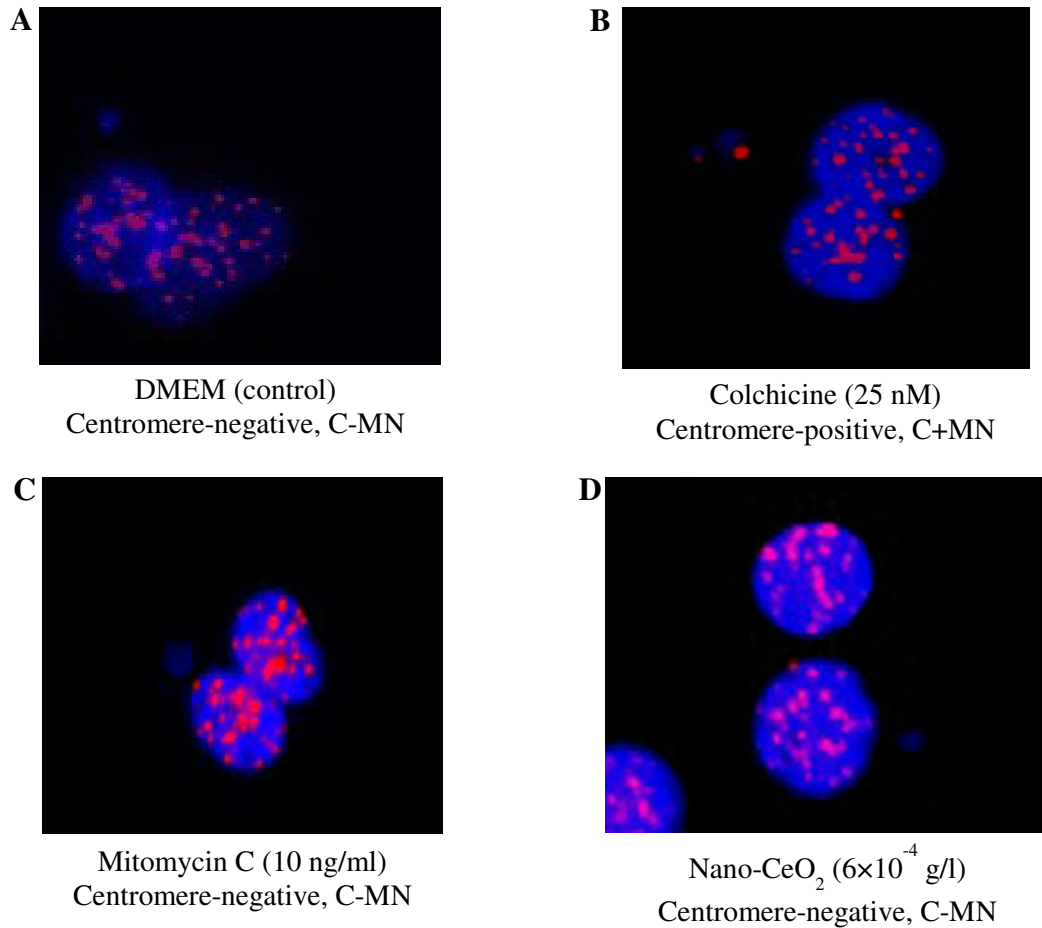


Figure 8. Typical fluorescent images of micronuclei in binucleated human dermal fibroblasts incubated for 48 h under indicated conditions. Images were acquired on an epifluorescence microscope (BX 60 Olympus) at 400X magnification.

## References :

Auffan M, Rose J, Orsière T, De Meo M, Thill A, Zeyons O, Proux O, Masion A, Chaurand P, Spalla O, Botta A, Wiesner MR, Bottero JY. 2009. CeO<sub>2</sub> nanoparticles induce DNA damage towards human dermal fibroblasts *in vitro*. *Nanotoxicology* 3:161–171.

Bianconi A, Marcelli A, Dexpert H, Karnatak R, Kotani A, Jo T, Petiau J. 1987. Specific intermediate-valence state of insulating 4f compounds detected by L<sub>3</sub> X-ray absorption. *Phys Rev B* 35:806–812.

De Faria LA, Trasatti S. 1994. The point of zero charge of CeO<sub>2</sub>. *J Colloid Interface Sci* 167:352–357.

Dexpert H, Karnatak RC, Esteva JM, Connerade JP, Gasgnier M, Caro PE, Albert L. 1987. X-ray absorption studies of CeO<sub>2</sub>, PrO<sub>2</sub>, and TbO<sub>2</sub>. II. Rare-earth valence state by L<sub>III</sub> absorption edges. *Phys Rev B* 36:1750–1753.

Finkelstein LD, Postnikov AV, Efremova NN, Kurmaev EZ. 1992. X-Ray Ce L<sub>III</sub> absorption in CeO<sub>2</sub> and BaCeO<sub>3</sub>: experiment and interpretation on the basis of LMTO band structure calculations. *Material Letters* 14:115–118.

Nabavi M, Spalla O, Cabane B. 1993. Surface chemistry of nanometric ceria particles in aqueous dispersion. *J Colloid Interface Sci* 160:459–471.

Takahashi Y, Sakami H, Nomura M. 2002. Determination of the oxidation state of cerium in rocks by Ce L<sub>III</sub>-edge X-ray absorption near-edge structure spectroscopy. *Anal Chim Acta* 468:345–354.

Thill A, Zeyons O, Spalla O, Chauvat F, Rose J, Auffan M, Flank AM. 2006. Cytotoxicity of CeO<sub>2</sub> nanoparticles for *Escherichia coli*. Physico-chemical insight of the cytotoxicity mechanism. *Environ Sci Technol* 40:6151–6156.